Monthly Notices
of the
ROYAL ASTRONOMICAL SOCIETY

MNRAS **445,** 2049–2060 (2014) doi:10.1093/mnras/stu1849

Milky Way mass constraints from the Galactic satellite gap

Marius Cautun,[1,2]★ Carlos S. Frenk,[1] Rien van de Weygaert,[2]
Wojciech A. Hellwing[1,3] and Bernard J. T. Jones[2]

[1]*Department of Physics, Institute for Computational Cosmology, University of Durham, South Road, Durham DH1 3LE, UK*
[2]*Kapteyn Astronomical Institute, University of Groningen, PO Box 800, NL-9747 AV Groningen, the Netherlands*
[3]*Interdisciplinary Centre for Mathematical and Computational Modellings, University of Warsaw, ul. Pawińskiego 5a, PL-02-106 Warsaw, Poland*

Accepted 2014 September 4. Received 2014 August 14; in original form 2014 May 29

ABSTRACT

We use the distribution of maximum circular velocities, $V_{\rm max}$, of satellites in the Milky Way (MW) to constrain the virial mass, M_{200}, of the Galactic halo under an assumed prior of a Λ cold dark matter universe. This is done by analysing the subhalo populations of a large sample of haloes found in the Millennium II cosmological simulation. The observation that the MW has at most three subhaloes with $V_{\rm max} \geq 30\ {\rm km\,s^{-1}}$ requires a halo mass $M_{200} \leq 1.4 \times 10^{12}\,{\rm M_\odot}$, while the existence of the Magellanic Clouds (assumed to have $V_{\rm max} \geq 60\ {\rm km\,s^{-1}}$) requires $M_{200} \geq 1.0 \times 10^{12}\,{\rm M_\odot}$. The first of these conditions is necessary to avoid the 'too-big-to-fail' problem highlighted by Boylan-Kolchin et al., while the second stems from the observation that massive satellites like the Magellanic Clouds are rare. When combining both requirements, we find that the MW halo mass must lie in the range $0.25 \leq M_{200}/(10^{12}\,{\rm M_\odot}) \leq 1.4$ at 90 per cent confidence. The gap in the abundance of Galactic satellites between $30\ {\rm km\,s^{-1}} \leq V_{\rm max} \leq 60\ {\rm km\,s^{-1}}$ places our galaxy in the tail of the expected satellite distribution.

Key words: Galaxy: abundances – Galaxy: halo – dark matter.

1 INTRODUCTION

Due to their proximity, the Milky Way (MW) and its satellite galaxies provide an unparalleled data set for testing astrophysical and cosmological ideas. For example, resolving the stellar content of the dwarf spheroidals enables tests of galaxy formation and evolution theory (Grebel 2005); analysing their internal kinematics constrains the nature of their dark matter content (e.g. Strigari, Frenk & White 2010); detecting satellites three orders of magnitude fainter than in external galaxies (e.g. Willman et al. 2005) provides information on the physics of extreme, very low luminosity galaxies. Given that the MW satellites play such a prominent role, it is important to investigate how representative the MW substructures are of systems of this kind.

Several alleged points of tension between observations and predictions of the standard cosmological model, Λ cold dark matter (ΛCDM), concern properties of the MW and its satellites. One is an apparent discrepancy between the predicted distribution of the maximum circular velocity, $V_{\rm max}$, of the most massive subhaloes and the inferred values for the MW satellites. This is often referred to as the 'satellite problem', and was originally identified by Klypin et al. (1999) and Moore et al. (1999). Another variant of this discrepancy was recently highlighted by Parry et al. (2012) and by Boylan-Kolchin, Bullock & Kaplinghat (2011b, 2012) who dubbed it the 'too-big-to-fail' (TBTF) problem.

Various arguments based on the kinematics of the nine bright 'classical' dwarf spheroidal satellites of the MW suggest that they reside in subhaloes with maximum circular velocities of $V_{\rm max} \lesssim 30\ {\rm km\,s^{-1}}$ (Peñarrubia, McConnachie & Navarro 2008; Strigari et al. 2008; Łokas 2009; Walker et al. 2009; Strigari et al. 2010; Wolf et al. 2010), or even $V_{\rm max} \lesssim 25\ {\rm km\,s^{-1}}$ (Boylan-Kolchin et al. 2012). If this is indeed the case, only the two Magellanic Clouds (MCs) and the Sagittarius dwarf would reside in dark matter substructures with larger maximum velocity than this. Using the Aquarius simulations (Springel et al. 2008), Boylan-Kolchin et al. (2011b, 2012) argued that having at most three massive satellites with $V_{\rm max} \geq 30\ {\rm km\,s^{-1}}$ in the MW is in conflict with current understanding of galaxy formation and evolution within ΛCDM: simulations produce, on average, eight, not three, subhaloes with $V_{\rm max}$ larger than $30\ {\rm km\,s^{-1}}$. At face value, this would require the most massive substructures to be devoid of stars when less massive objects are not. This is not expected in models of how galaxies populate low-mass haloes (e.g. Benson et al. 2002) and could signal a fundamental shortcoming of the ΛCDM model itself. A similar conclusion was independently reached by Parry et al. (2012) from hydrodynamic simulations of galaxy formation in some of the Aquarius haloes.

★ E-mail: marius.cautun@gmail.com

A possible solution to the TBTF problem was put forward by Wang et al. (2012, hereafter Wang12). Using the approximate invariance of the scaled subhalo maximum velocity function with host halo mass (see e.g. Moore et al. 1999; Kravtsov et al. 2004; Zheng et al. 2005; Springel et al. 2008; Weinberg et al. 2008), Wang12 derived statistics for galactic subhaloes and estimated the probability that an MW halo contains three or fewer satellites with $V_{\rm max} \geq 30$ km s^{-1}, as a function of the host halo mass. These results were further refined by Cautun et al. (2014, hereafter C14), who developed a better method for estimating the abundance of galactic subhaloes in cosmological simulations. Both studies found that rather than ruling out ΛCDM, the small number of massive satellites in our galaxy imposes an upper limit to the mass of the MW halo if ΛCDM is the correct model. They found that the MW satellite data are consistent with ΛCDM predictions at the 10 per cent confidence level if the MW halo has a virial mass $<1.3 \times 10^{12}$ M$_\odot$, which is near the lower end of commonly accepted values. A similar solution to the TBTF problem was proposed by Purcell & Zentner (2012), who compared the structure of MW satellites with that of subhaloes predicted by a semi-analytical model. They recognized that the solution to the problem requires the mass of the MW halo to be below a certain value that, however, is significantly larger than the value we find in this paper.

A low MW halo mass, however, has a large impact on the probability of finding the two MCs, which are rather massive. Recent estimates with *Hubble Space Telescope* data find maximum circular velocities of (92 ± 19) km s^{-1} and (60 ± 5) km s^{-1} for the Large and Small MCs, respectively, (Kallivayalil et al. 2013; van der Marel & Kallivayalil 2014), which broadly agree with measurements based on H I and stellar kinematics (e.g. van der Marel et al. 2002; Stanimirović, Staveley-Smith & Jones 2004; Harris & Zaritsky 2006; Olsen & Massey 2007). Simulation studies agree that, in ΛCDM, substructures with the mass of the MCs are common in massive galactic haloes, of mass $\sim$2–3 $\times$ 10^{12} M$_\odot$, but are quite rare in haloes of lower mass, $\lesssim 1 \times 10^{12}$ M$_\odot$ (Boylan-Kolchin, Besla & Hernquist 2011a; Busha et al. 2011a,b; González, Kravtsov & Gnedin 2013). Galaxy redshift survey data indicate that galaxies with luminosity similar to the MW have $\sim$4 per cent probability of hosting two satellites like the MCs (Guo et al. 2011; Lares, Lambas & Domínguez 2011; Liu et al. 2011). Taking into account both mass and orbital data for the two MCs, Busha et al. (2011a) and González et al. (2013a) estimate a mass of $\sim 1.2 \times 10^{12}$ M$_\odot$ for the MW halo, in contradiction with the conclusion of Boylan-Kolchin et al. (2011a), which, using similar considerations, found that the MW halo mass is unlikely to be less than 2×10^{12} M$_\odot$. The former is consistent with the constraint of Wang12 but the latter is not.

In this paper, we investigate the constraints that the massive satellite population of the MW sets on the mass of its dark matter halo in the context of the ΛCDM model. In addition, we remark on the peculiar gap in the number of satellites in the MW, with at most one satellite in the range $30 \leq V_{\rm max} \leq 60$ km s^{-1}. The TBTF problem is predicated on the basis of this gap. Such gaps are rare in our simulations and might signal a tension between the ΛCDM model and observations. However, it is not clear how an a posteriori argument of this nature can be put on a proper statistical basis. This study was possible by making use of a large and representative sample of simulated haloes for which we determine the subhalo number statistics down to $V_{\rm max} \sim 15$ km s^{-1} using the extrapolation method presented in C14.

The remainder of this paper is organized as follows. In Section 2, we give a description of the simulations and of the method we employ to extend the dynamic range over which we derive subhalo count statistics. In Section 4, we calculate the probability of finding MW-like subhaloes as a function of halo mass. In Section 5, we examine the sensitivity of our results to model parameters. We conclude in Section 6 with a brief summary of our main results.

2 THE SIMULATIONS

We make use of the high-resolution Millennium-II cosmological *N*-body simulation (MS-II; Boylan-Kolchin et al. 2009). MS-II follows the evolution of CDM, using 2160^3 particles to resolve structure formation in a periodic cube $100\,h^{-1}$ Mpc on a side. Each particle has a mass, $m_{\rm p} = 9.44 \times 10^6$ M$_\odot$, so MW-sized haloes ($\sim 10^{12}$ M$_\odot$) are resolved with $\sim 10^5$ particles. This represents a good compromise between having a representative sample of MW-like haloes and resolving the most massive 10 substructures per host halo. The spatial resolution is given by the Plummer-equivalent force softening, $\epsilon = 1\,h^{-1}$ kpc, which was kept constant in comoving coordinates for the entire simulation. MS-II uses the *Wilkinson Microwave Anisotropy Probe* 1 (*WMAP*-1) cosmogony (Spergel et al. 2003) with the following cosmological parameters: $\Omega_{\rm m} = 0.23$, $\Omega_\Lambda = 0.75$, $h = 0.73$, $n_{\rm s} = 1$ and $\sigma_8 = 0.9$.

2.1 Halo finder

Haloes and subhaloes in the simulation were identified with the ROCKSTAR (Robust Overdensity Calculation using K-Space Topologically Adaptive Refinement) phase-space halo finder (Behroozi, Wechsler & Wu 2013). ROCKSTAR starts by selecting potential haloes as Friends-of-Friends (FOF) groups in position space using a large linking length ($b = 0.28$). This first step is restricted to position space to optimize the use of computational resources, while each subsequent step is carried out using the full 6D phase-space information. Each FOF group from the first step is used to create a hierarchy of FOF phase-space subgroups by progressively reducing the linking length. The phase-space subgroups are selected with an adaptive phase-space linking length such that each successive subgroup has 70 per cent of the parent's particles. ROCKSTAR uses the resulting subgroups as potential halo and subhalo centres and assigns particles to them based on their phase-space proximity. Once all particles are assigned to haloes and subhaloes, an unbinding procedure is applied to keep only the gravitationally bound particles. The final halo centres are computed from a small region around the phase-space density maximum associated with each object.

The outer boundary of the haloes is cut at the point where the enclosed overdensity decreases below $\Delta = 200$ times the critical density, $\rho_{\rm c}$. Therefore, the halo mass, M_{200}, and radius, R_{200}, correspond to a spherical overdensity of $200\rho_{\rm c}$. Using this definition of the main halo boundaries we define the satellite population as all the subhaloes within a distance, R_{200}, from the host centre.

2.2 Subhalo number statistics

A challenge when studying galactic substructures in simulations is to achieve the large dynamic range required for all subhaloes above a certain threshold ($V_{\rm max} \geq 30$ km s^{-1} in our case) to be resolved for a statistically useful sample. One strategy is to run ensembles of very high resolution simulations of galactic haloes. (e.g. Diemand et al. 2008; Madau, Diemand & Kuhlen 2008; Springel et al. 2008; Stadel et al. 2009). However, the limited sample size, six in the Aquarius programme, the largest to date, limits the extent to which they can be used to study how common the MW satellite systems are. The alternative strategy is to run simulations of cosmological

volumes that produce representative samples of galactic haloes, but are limited in resolution, so that not all the subhaloes above the desired $V_{\rm max}$ threshold are resolved (Boylan-Kolchin et al. 2009; Klypin, Trujillo-Gomez & Primack 2011). For example, while MS-II captures all substructures with $V_{\rm max} \geq 45$ km s^{-1}, it only generates an incomplete population of less massive subhaloes (see C14). To be able to use MS-II for our analysis we need to recover the full population of substructures down to at least $V_{\rm max} = 30$ km s^{-1}. We now summarize a procedure introduced in C14 for achieving this.

We are interested in the subhalo abundance as a function of the ratio,

$$\nu = \frac{V_{\rm max}}{V_{200}}, \quad (1)$$

between the subhalo maximum velocity, $V_{\rm max}$, and the virial velocity, V_{200}, of the host halo. We use this quantity to characterize the halo population because the maximum velocity provides a robust measurement of subhalo size that is independent of the identification algorithm and definition of subhalo boundary (for details see Onions et al. 2012). Moreover, since $V_{\rm max}$ depends only on the mass distribution in the central parts of the object, it allows for a closer comparison with observations that typically probe only the inner regions of a halo where the galaxy resides. We now quantify the statistics of the number of subhaloes exceeding ν and consider both the mean subhalo count, $\overline{N}(>\nu)$, and the dispersion, $\sigma(>\nu)$.

The effects of limited resolution on the subhalo number counts are illustrated in Fig. 1. It contrasts, as a function of ν, the mean subhalo count of (0.8–1.8) $\times$ 10^{13} M$_\odot$ mass haloes resolved at low resolution in the Millennium simulation (Springel et al. 2005) and at 125 times higher mass resolution in the MS-II (reproduced from C14). The low-resolution calculation recovers the massive substructures, but only finds a partial population of subhaloes below $\nu \approx 0.4$. While the exact value of ν below which a given simulation misses subhaloes depends on several parameters, especially the number of particles used to resolve the host halo, the qualitative behaviour shown in Fig. 1 holds for a wide range of halo masses.

The subhalo population statistics, $\overline{N}(>\nu)$ and $\sigma(>\nu)$, can be recovered to up to three times lower values of ν than is possible in the simulation itself by using the extrapolation method described in C14. The first step consists of quantifying how many substructures are missing at each value of ν in a given sample of equal mass haloes. Once this is known, the method adds the missing subhaloes using a probabilistic approach. Each new subhalo is randomly assigned to one of the haloes in the sample. This procedure recovers the subhalo statistics, but not the substructure of individual haloes or their spatial distribution.

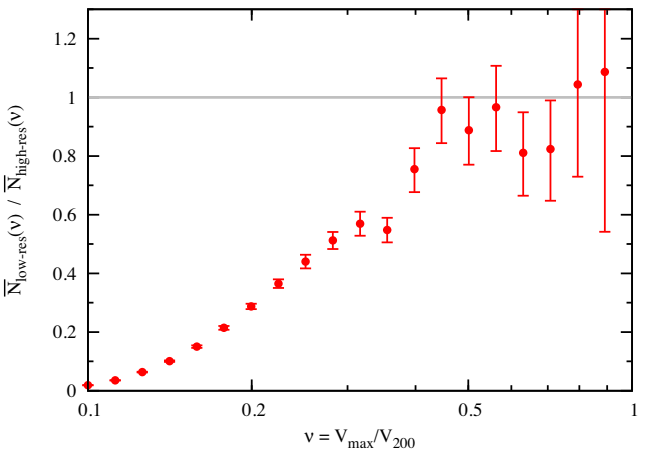

Figure 1. The impact of numerical resolution on the number of subhaloes found in simulations. The plot shows the ratio, $\overline{N}_{\rm low-res}(\nu)/\overline{N}_{\rm high-res}(\nu)$, between the mean subhalo count in a low- and a high-resolution simulation. A ratio of one corresponds to recovering the full substructure population, while lower values reflect missing subhaloes in the low-resolution simulation. Reproduced from C14.

By applying our extrapolation method to the MS-II data, in C14 we studied the subhalo number statistics down to substructures with $V_{\rm max} \sim 15$ km s^{-1}. Here, we summarize some of the results of C14 that are of importance to the present study. In C14, we have found that the probability distribution function (PDF) of the number of subhaloes exceeding ν is well modelled by a negative binomial distribution (see also Boylan-Kolchin et al. 2010),

$$P(N|r,s) = \frac{\Gamma(N+r)}{\Gamma(r)\Gamma(N+1)} s^r (1-s)^N , \quad (2)$$

where $\Gamma(x) = (x-1)!$ denotes the Gamma function. The parameters, r and s, are given in terms of the mean, $\overline{N}(>\nu)$, and the variance, $\sigma^2(>\nu)$, of the subhalo population by

$$r(>\nu) = \frac{\overline{N}^2(>\nu)}{\sigma^2(>\nu) - \overline{N}(>\nu)} \quad \text{and} \quad s(>\nu) = \frac{\overline{N}(>\nu)}{\sigma^2(>\nu)} . \quad (3)$$

To obtain the substructure number distribution functions, we employ the mean and the dispersion of the subhalo population computed in C14. While in C14, these quantities were computed for haloes in the mass range (0.8–3) $\times$ 10^{12} M$_\odot$, the results are largely independent of the exact halo mass (see C14 and Fig. 4).

3 LIMITS ON THE MW HALO MASS

In this section, we use the subhalo statistics of galactic haloes to constrain the mass of the MW halo assuming the ΛCDM model. As we discussed in the introduction, various studies suggest that in the MW only the two MCs and the Sagittarius dwarf reside in haloes of maximum circular velocity, $V_{\rm max} \geq 30$ km s^{-1}. H I and stellar kinematics data suggest that the subhaloes of the MCs have $V_{\rm max} \geq 60$ km s^{-1} (Kallivayalil et al. 2013). Therefore, the MW has at most three subhaloes with $V_{\rm max} \geq 30$ km s^{-1} and at least two with $V_{\rm max} \geq 60$ km s^{-1}. We denote such a population of substructures as an *MW-like subhalo system*.

We first obtain the fraction of haloes containing three or fewer subhaloes with $V_{\rm max} \geq 30$ km s^{-1} in the ΛCDM model and, following Wang12, use this to set an upper limit to the MW halo mass. We then independently obtain the probability that a halo has at least two substructures with $V_{\rm max} \geq 60$ km s^{-1} and set a lower limit on the MW halo mass.

3.1 An upper limit to the MW halo mass

The negative binomial distribution, $P(k|r(>\nu_0), s(>\nu_0))$, of equation (2) gives the PDF that a halo has k subhaloes with velocity ratio exceeding $\nu_0 \equiv V_0/V_{200}$. It is then straightforward to estimate the probability that a halo has at most X substructures with $V_{\rm max} \geq V_0$. This is simply the fraction of haloes that have at most X subhaloes with $\nu \geq \nu_0$ and can be obtained by summing over the subhalo abundance PDF at ν_0,

$$p(\leq X, V_0) = \sum_{k=0}^{X} P(k|r(>\nu_0), s(>\nu_0)) \quad \text{with } \nu_0 = \frac{V_0}{V_{200}} . \quad (4)$$

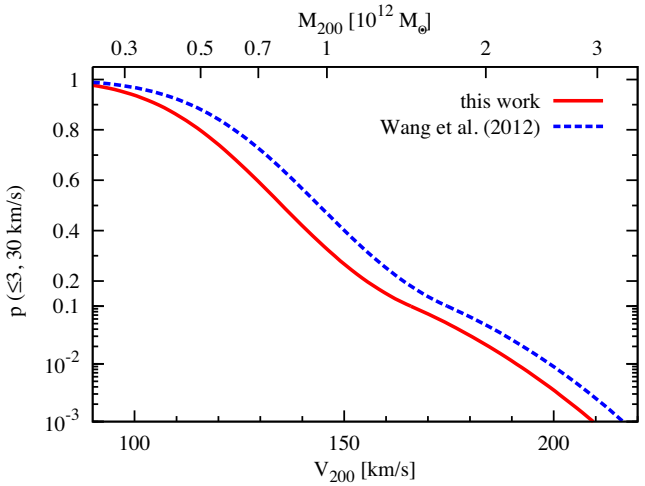

Figure 2. The probability, $p(\leq 3, 30\ \mathrm{km\,s^{-1}})$, that a halo contains at most three subhaloes with $V_{\rm max} \geq 30\ \mathrm{km\,s^{-1}}$ as a function of the host virial velocity, V_{200}, (lower tick marks) and virial mass, M_{200}, (upper tick marks). The solid curve gives our results, while the dashed line shows the previous results of Wang12. Note that the y-axis is linear above 0.1 and logarithmic for lower values.

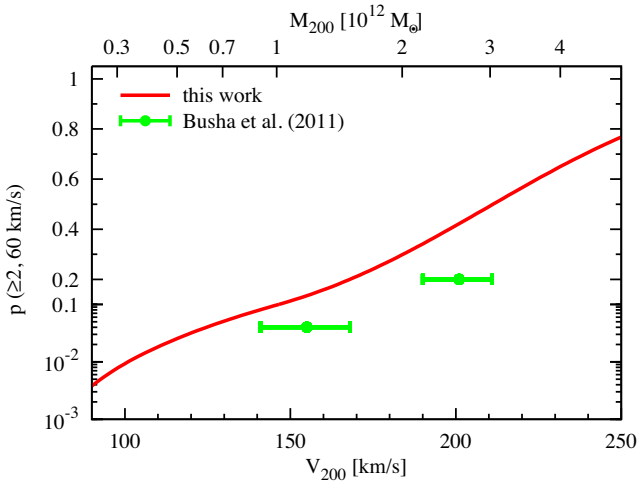

Figure 3. The probability, $p(\geq 2, 60\ \mathrm{km\,s^{-1}})$, that a halo contains at least two subhaloes with $V_{\rm max} \geq 60\ \mathrm{km\,s^{-1}}$ as a function of the host virial velocity, V_{200}, (lower axis), and virial mass, M_{200}, (upper axis). The solid curve shows our predictions, while the filled circles show the results of Busha et al. (2011b). Note that the y-axis is linear above 0.1 and logarithmic for lower values.

Table 1. The fraction of MS-II haloes with massive subhaloes similar to those of the MW. The table lists the probability, $p(\leq 3, 30\ \mathrm{km\,s^{-1}})$, of finding at most three subhaloes with $V_{\rm max} \geq 30\ \mathrm{km\,s^{-1}}$, and the probability, $p(\geq 2, 60\ \mathrm{km\,s^{-1}})$, of finding at least two subhaloes with $V_{\rm max} \geq 60\ \mathrm{km\,s^{-1}}$. The last row gives the combined probability of satisfying both conditions simultaneously.

Halo mass	$(\times 10^{12}\ \mathrm{M_\odot})$	0.5	0.7	1	2
$p(\leq 3, 30\ \mathrm{km\,s^{-1}})$	(per cent)	80	59	33	2.3
$p(\geq 2, 60\ \mathrm{km\,s^{-1}})$	(per cent)	2.2	4.7	10	30
$p(\geq 2, 60\ \mathrm{km\,s^{-1}}; \leq 3, 30\ \mathrm{km\,s^{-1}})$	(per cent)	0.8	0.7	0.4	0.04

The distribution parameters, $r(>\nu)$ and $s(>\nu)$, are uniquely determined by the mean $\overline{N}(>\nu)$ and scatter $\sigma(>\nu)$ of the subhalo population via equation (3).

The fraction of galactic haloes, $p(\leq 3, 30\ \mathrm{km\,s^{-1}})$, with at most three subhaloes with $V_{\rm max} \geq 30\ \mathrm{km\,s^{-1}}$ is given in Fig. 2 as a function of the host virial velocity, V_{200} (lower tick marks), and, equivalently, host virial mass, M_{200} (upper tick marks). For clarity, we plot the halo fraction on a linear scale for values larger than 0.1 and on a logarithmic scale for smaller values. The probability of having at most three subhaloes with $V_{\rm max} \geq 30\ \mathrm{km\,s^{-1}}$, shown as a thick red curve, is a steep function of host mass, decreasing from 33 per cent at $10^{12}\ \mathrm{M_\odot}$ to 0.1 per cent at $3 \times 10^{12}\ \mathrm{M_\odot}$. For convenience, we summarize the probabilities for indicative halo masses in Table 1. Under the assumption that ΛCDM is the correct model, our results then imply a 90 per cent confidence upper limit of $1.4 \times 10^{12}\ \mathrm{M_\odot}$ for the virial mass of the MW halo, M_{200}; a mass of $2 \times 10^{12}\ \mathrm{M_\odot}$ is ruled out at 97.7 per cent confidence.

The probability of finding at most three haloes with $V_{\rm max} \geq 30\ \mathrm{km\,s^{-1}}$ as a function of V_{200} was previously derived by Wang12 whose results are shown by the dashed curve in Fig. 2. We find slightly lower upper limits than them for the mass of the MW halo because they underestimated the subhalo mass at which resolution effects become important. As a result, they found 20 per cent fewer substructures than we do (see C14 for more details), causing them to overestimate $p(\leq 3, 30\ \mathrm{km\,s^{-1}})$ at a given halo mass.

3.2 A lower limit to the MW halo mass

The fraction of haloes which have at least X subhaloes with $V_{\rm max} \geq V_0$ can be expressed as

$$p(\geq X, V_0) = 1 - p(\leq X-1, V_0)\,, \tag{5}$$

with $p(\leq X-1, V_0)$ given by equation (4).

The probability, $p(\geq 2, 60\ \mathrm{km\,s^{-1}})$, of a halo hosting at least two subhaloes with $V_{\rm max} \geq 60\ \mathrm{km\,s^{-1}}$ is shown as a solid curve in Fig. 3. This represents the fraction of haloes that host MCs-like or more massive substructures as a function of the V_{200} or M_{200} of the host halo. This probability is small in low-mass haloes but increases rapidly towards more massive hosts. Therefore, assuming ΛCDM, $p(\geq 2, 60\ \mathrm{km\,s^{-1}})$ sets a lower limit on the MW halo mass. From Fig. 3, we find a lower limit of $1.0 \times 10^{12}\ \mathrm{M_\odot}$ for the mass of the MW halo at 90 per cent confidence.

The probability of finding two or more substructures with $V_{\rm max} \geq 60\ \mathrm{km\,s^{-1}}$ in galactic haloes was previously estimated by Busha et al. (2011b) whose results are shown as filled circles in Fig. 3. Our values are a factor of a few higher than theirs. We suspect that the difference arises because Busha et al. (2011b) used the Bolshoi simulation (Klypin et al. 2011) which misses a large number of MCs-like substructures due to numerical resolution effects. Bolshoi has approximatively the same number of dark matter particles as MS-II, but a volume ∼15 times larger. Given that MS-II misses subhaloes with $V_{\rm max} < 45\ \mathrm{km\,s^{-1}}$ (see C14), we suspect that the Bolshoi simulation underestimates the number of substructures with $V_{\rm max}$ below $45\ \mathrm{km\,s^{-1}} \times 15^{1/3} \sim 100\ \mathrm{km\,s^{-1}}$.

4 THE MASS DISTRIBUTION OF THE MW

In this section, we estimate the mass of the MW, given that our galaxy contains at most three subhaloes with $V_{\rm max} \geq 30\ \mathrm{km\,s^{-1}}$, out of which two have at least $V_{\rm max} \geq 60\ \mathrm{km\,s^{-1}}$, to which we refer as an MW-like subhalo system. A crucial ingredient of this analysis is the correlation between the presence of satellites with $V_{\rm max} \geq 60\ \mathrm{km\,s^{-1}}$ and those with $V_{\rm max} \geq 30\ \mathrm{km\,s^{-1}}$, which we estimate from cosmological simulations. This is in contrast to the results of the previous

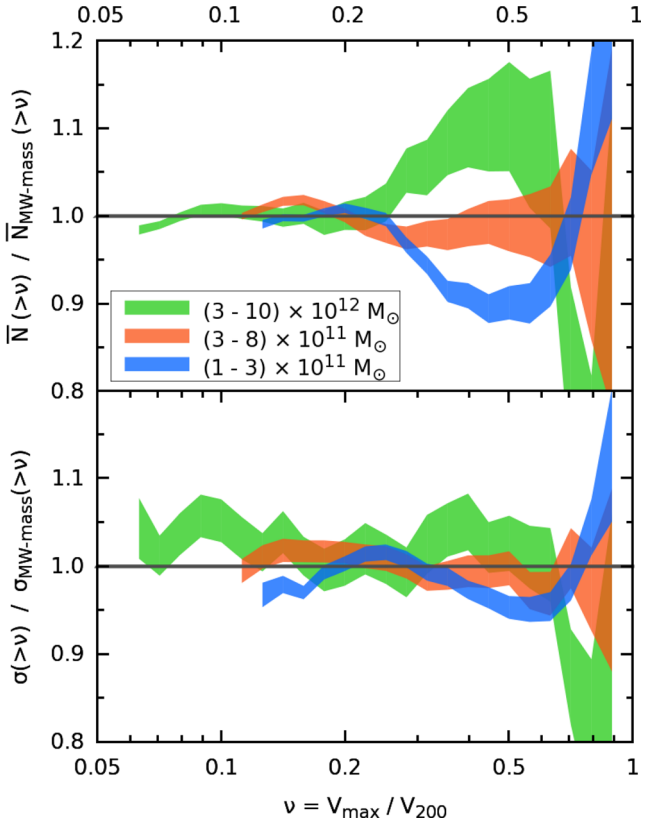

Figure 4. The mean, $\overline{N}(>\nu)$ (top panel), and the dispersion, $\sigma(>\nu)$ (lower panel), of the subhalo abundance as a function of velocity ratio, ν, for haloes in different mass bins. For clarity, we plot the ratio with respect to the values for haloes in the mass range (0.8–3) × 10^{12} $M_\odot$. A ratio of 1 corresponds to no variation with host mass. The vertical width of the curves shows the bootstrap error associated with $\overline{N}(>\nu)$ and $\sigma(>\nu)$.

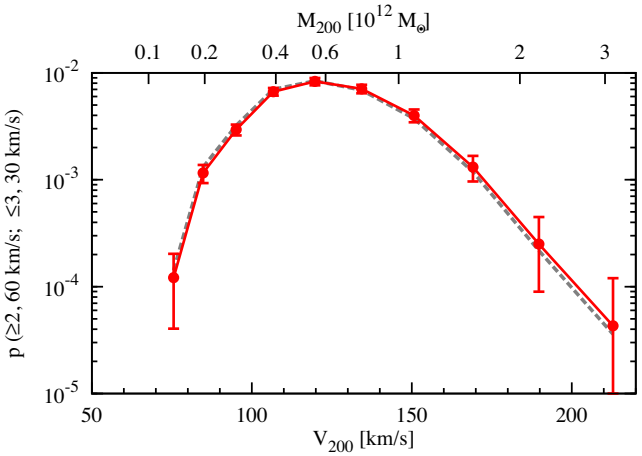

Figure 5. The probability, $p(\geq 2, 60\ \mathrm{km\,s^{-1}};\ \leq 3, 30\ \mathrm{km\,s^{-1}})$, that a halo has an MW-like subhalo population as a function of halo virial velocity (lower tick marks) and virial mass (upper tick marks). The error bars show the 1σ spread due to the finite number of haloes and different realizations of the subhalo extrapolation method. The dashed grey line shows the size of the shift towards lower V_{200} values when multiplying the probability by the halo mass function. Note the logarithmic y-axis.

section which treated the two satellite populations as independent, which is clearly not the case.

To obtain the mass distribution of haloes that contain MW-like satellite systems, we compute the probability, $p(\geq X_1, V_1;\ \leq X_2, V_2)$, that a halo contains at least X_1 subhaloes with $V_{max} \geq V_1$ and at most X_2 substructures with $V_{max} \geq V_2$. As we shall see later, this probability is quite small for the kind of MW subhaloes of interest here and thus a large sample of haloes is required for a robust estimate. Due to its limited volume, the MS-II does not provide sufficient statistics for galactic haloes.

Following Wang12, we can overcome this limitation by appealing to the approximate invariance of the scaled subhalo velocity function, $\overline{N}(>\nu)$, with host halo mass, that is, to the fact that, to good approximation, the subhalo number PDF is independent of halo mass when expressed as a function of ν (Moore et al. 1999; Kravtsov et al. 2004; Zheng et al. 2005; Springel et al. 2008; Weinberg et al. 2008; Wang12; C14). This is clearly seen in Fig. 4 which compares the mean and the dispersion of the subhalo number counts in haloes of different mass. We take haloes in the mass range (0.8–3) × 10^{12} $M_\odot$ as reference since this interval encompasses the likely value for the MW as seen in the preceding section and also as argued by e.g. Battaglia et al. (2005), Dehnen, McLaughlin & Sachania (2006), Xue et al. (2008), Gnedin et al. (2010), Guo et al. (2010). The figure shows that, to (10–20) per cent accuracy, the number of substructures is independent of host halo mass over the mass range 10^{11}–10^{13} $M_\odot$.

To proceed further, we rewrite the probability in terms of constraints on the velocity ratio, ν. Given a halo of virial velocity, V_{200}, we define

$$\nu_1 = \frac{V_1}{V_{200}} \quad \text{and} \quad \nu_2 = \frac{V_2}{V_{200}}\,. \tag{6}$$

Computing $p(\geq X_1, V_1;\ \leq X_2, V_2)$ now reduces to finding the probability that a halo contains at least X_1 subhaloes with $\nu \geq \nu_1$ and at most X_2 subhaloes with $\nu \geq \nu_2$.

The probability of finding a MW-like substructure population in the MS-II is given in Fig. 5 as a function of both halo virial velocity and halo mass. The probability has a peak value of ∼1 per cent, i.e. at most one out of 100 haloes of that mass has an MW-like subhalo population. Thus, satellite systems such as the one in our galaxy are rare in a ΛCDM universe.

The rarity of the MW subhalo population depends strongly on the mass of the MW halo. The probability is largest for haloes in the mass range ∼(0.4–1.0) × 10^{12} $M_\odot$ and drops off sharply outside this interval, decreasing below one-tenth of its peak value outside the mass range (0.2–1.5) × 10^{12} $M_\odot$.

To constrain the MW halo mass, we need to multiply the probability of finding an MW-like subhalo system in a halo of a given mass, $p(\geq 2, 60\ \mathrm{km\,s^{-1}};\ \leq 3, 30\ \mathrm{km\,s^{-1}})$, by the total number of haloes of that mass. This gives the mass distribution of haloes with MW-like satellite systems.[1] Due to the sharp drop of the probability outside its peak, multiplying by the halo mass function results only in a slight shift of the distribution to lower halo masses. This is shown by the dashed grey line in Fig. 5. This shift is negligible in comparison to other uncertainties, as we discuss in Section 5, and, to a good approximation, can be neglected.

To obtain the new MW mass constraints, we identify the region under the $p(\geq 2, 60\ \mathrm{km\,s^{-1}};\ \leq 3, 30\ \mathrm{km\,s^{-1}})$ curve that contains 90 per cent of the area. This gives an MW mass range of (0.25–1.4) × 10^{12} $M_\odot$, at 90 per cent confidence, with a most likely value

[1]This is equivalent to taking a flat prior over halo masses, which is the simplest prior to assume.

of $0.6 \times 10^{12}\,\mathrm{M}_\odot$ given by the peak of the distribution. While the upper limit is the same as we found earlier using the halo fraction, $p(\leq 3, 30\ \mathrm{km\,s^{-1}})$, the lower mass limit is significantly lower than the $1.0 \times 10^{12}\,\mathrm{M}_\odot$ value inferred from the $p(\geq 2, 60\ \mathrm{km\,s^{-1}})$ analysis. Thus, treating the MW satellite numbers with $V_{\rm max} \geq 60\ \mathrm{km\,s^{-1}}$ and $V_{\rm max} \geq 30\ \mathrm{km\,s^{-1}}$ independently of each other gives a Galactic mass range that is both narrower and centred at larger values.

In Fig. 6, we illustrate a few examples of haloes that could potentially contain an MW-like subhalo population.[2] We find candidate haloes with a wide range of masses and embedded in a variety of large-scale environments. For example, the haloes in panels (a) and (c) do not have similarly massive neighbours in their vicinity, while the halo in panel (b) is part of a group with at least one more massive member. Substructures with $V_{\rm max} \geq 20\ \mathrm{km\,s^{-1}}$ found within the virial radius of each object are marked with solid circles. Even though each of the four haloes has at most three massive satellites, they contain tens of subhaloes with $20\ \mathrm{km\,s^{-1}} \leq V_{\rm max} \leq 30\ \mathrm{km\,s^{-1}}$ that can host the MW dwarf spheroidal satellites.

4.1 A model for the probability of having an MW-like subhalo population

In this section, we introduce a theoretical model that makes use of subhalo population statistics to predict the probability that a halo contains a population of substructures similar to that of our galaxy. This model is useful for exploring how the conclusions of the previous section depend on the assumed values of its parameters.

For example, given that at most 1 per cent of haloes at any mass have MW-like subhaloes, investigating $p(\geq 2, 60\ \mathrm{km\,s^{-1}};\ \leq 3, 30\ \mathrm{km\,s^{-1}})$ for a different cosmological model requires the analysis of $\sim 10^4$ MW-mass haloes and their substructures, which is a considerable computational effort. In contrast, obtaining robust subhalo population statistics can be done using a smaller number of haloes, and therefore the same outcome can be obtained much faster and cheaper.

We are interested in an analytical model that describes the probability for a halo to contain at least two substructures with $\nu \geq \nu_1$ and at most three substructures with $\nu \geq \nu_2$. The only hosts that contribute to this probability are those that have

(i) two subhaloes with $\nu \geq \nu_1$ and 0 or 1 with $\nu \in [\nu_2, \nu_1]$ or
(ii) three subhaloes with $\nu \geq \nu_1$ and 0 with $\nu \in [\nu_2, \nu_1]$.

Assuming that the number of subhaloes in the interval $[\nu_2, \nu_1]$ is independent of the number of subhaloes above ν_1, the contribution of each of the above two terms is given by

$$P(k|r(>\nu_1), s(>\nu_1)) \times P_{\rm Poisson}(\leq l)\ . \tag{7}$$

The first part of the equation is the negative binomial distribution that gives the fraction of haloes that contain k subhaloes with $\nu \geq \nu_1$ (see equation 2). The second part is the probability that a host contains at most l subhaloes in the interval $[\nu_2, \nu_1]$. This we model using a Poisson distribution, $P_{\rm Poisson}(\leq l)$. In the range $[\nu_2, \nu_1]$ each halo contains on average

$$\Delta N = \overline{N}(>\nu_2) - \overline{N}(>\nu_1) \tag{8}$$

[2]These haloes correspond to one realization of the subhalo extrapolation method. Since the method includes a random element, it cannot recover the substructures of an individual halo and so we can only identify potential candidates.

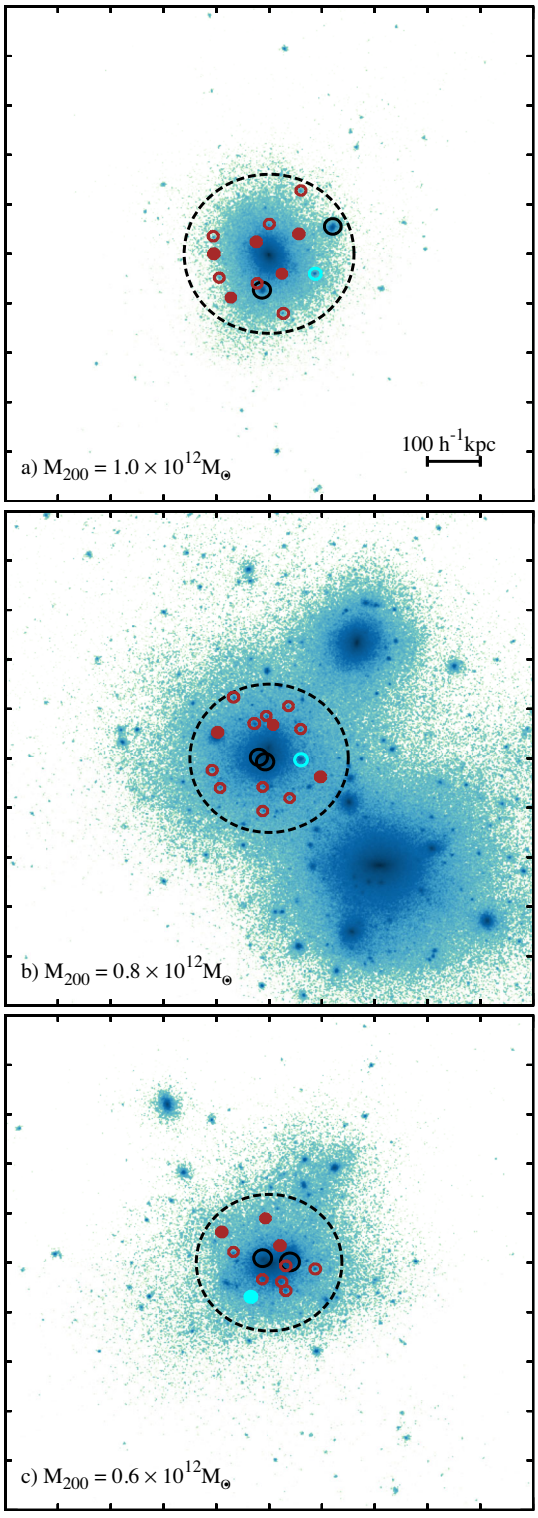

Figure 6. Examples of MS-II haloes that have a similar subhalo population to the MW. Each panel shows a $1 \times 1 \times 0.5\ (h^{-1}\ \mathrm{Mpc})^3$ projection centred on the halo. The black dashed circle indicates the virial radius. The solid circles inside the virial radius mark substructures with: $V_{\rm max} \geq 60\ \mathrm{km\,s^{-1}}$ (black), $30\ \mathrm{km\,s^{-1}} \leq V_{\rm max} \leq 60\ \mathrm{km\,s^{-1}}$ (cyan) and $20\ \mathrm{km\,s^{-1}} \leq V_{\rm max} \leq 30\ \mathrm{km\,s^{-1}}$ (dark red). The empty circles correspond to subhaloes found in the simulation, while the filled circles correspond to subhaloes added by our extrapolation method to compensate for numerical resolution effects.

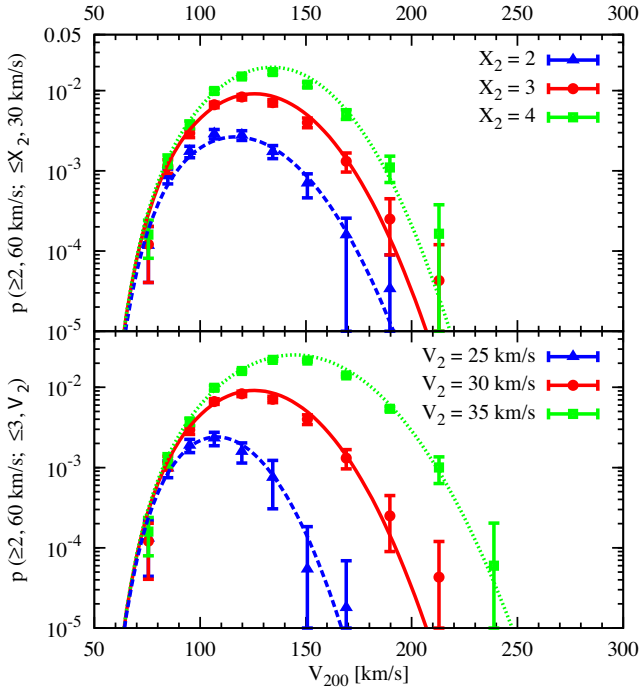

Figure 7. Comparison of our theoretical model with results from the MS-II simulations for the probability, $p(\geq X_1, V_1; \leq X_2, V_2)$, that a halo contains at least X_1 subhaloes with $V_{\rm max} \geq V_1$ and at most X_2 substructures with $V_{\rm max} \geq V_2$. We investigate departures from the default case, $p(\geq 2, 60\ {\rm km\,s^{-1}}; \leq 3, 30\ {\rm km\,s^{-1}})$. In the top panel, X_2 is varied while in the bottom panel V_2 is varied. The data points with bootstrap errors show the simulation results while the curves show the model predictions.

subhaloes. Assuming that this number follows a Poisson distribution with mean ΔN, the probability that a halo has l subhaloes in the interval $[\nu_2, \nu_1]$ is given by

$$\frac{\Delta N^l}{l!} {\rm e}^{-\Delta N} \ . \tag{9}$$

Putting everything together, we obtain the probability, $p(\geq 2, 60\ {\rm km\,s^{-1}}; \leq 3, 30\ {\rm km\,s^{-1}})$, of finding a halo with a subhalo population similar to that in the MW, which is given by

$$\sum_{k=2}^{3} P(k|r(>\nu_1), s(>\nu_1)) \sum_{l=0}^{3-k} \frac{\Delta N^l}{l!} {\rm e}^{-\Delta N} \ . \tag{10}$$

We refer to Appendix A for a derivation of the model and its predictions for the more general case of $p(\geq X_1, V_1; \leq X_2, V_2)$.

The subhalo number PDF diverges from a Poisson distribution for large values of $\overline{N}(>\nu)$ (Boylan-Kolchin et al. 2010, C14) and therefore our model gives only an approximate estimate of the true probability. A more realistic description would involve the use of a negative binomial distribution to characterize the probability for a halo to have l subhaloes in the range $[\nu_2, \nu_1]$, but at the expense of introducing an additional parameter. Since the deviation from a Poisson distribution is small for $\nu \gtrsim 0.15$ (C14), which defines the region of interest here, we expect that our model gives a good approximation to the probability of finding MW-like subhalo populations.

In Fig. 7, we compare the predictions of our model to the results obtained from the MS-II simulation. Since we are interested in the probability of MW-like subhalo populations, we explore a few representative examples close to this default case. In the top panel, we vary the number of subhaloes, X_2, and in the right-hand panel the velocity threshold, V_2. For all cases, we find that the model predictions and the simulation data agree very well, showing that our model gives a good approximation to the probability of finding MW-like subhalo systems.

5 DISCUSSION

The $V_{\rm max}$ distribution of the MW's most massive satellites places strong constraints on the mass of the MW halo given the prior hypothesis that ΛCDM is the correct model. In this case, the fact that the MW has only three satellites with $V_{\rm max} \geq 30\ {\rm km\,s^{-1}}$ (the two MCs and Sagittarius) requires the virial mass of the MW halo to be $M_{200} < 1.4 \times 10^{12}\ {\rm M_\odot}$ at 90 per cent confidence; on the other hand, the existence of the two MCs, which have $V_{\rm max} \geq 60\ {\rm km\,s^{-1}}$, requires $M_{200} > 1.0 \times 10^{12}\ {\rm M_\odot}$, also at 90 per cent confidence. This conclusion is consistent with some, but not all, recent measurements of the MW mass (Battaglia et al. 2005; Smith et al. 2007; Xue et al. 2008; Guo et al. 2010; Watkins, Evans & An 2010; Busha et al. 2011a; González, Kravtsov & Gnedin 2014; Diaz et al. 2014; Piffl et al. 2014).

These mass constraints were derived by treating the number of Galactic satellites with $V_{\rm max} \geq 60\ {\rm km\,s^{-1}}$ and those with $V_{\rm max} \geq 30\ {\rm km\,s^{-1}}$ as independent, which is clearly not the case. To overcome this, we defined haloes with MW-like subhalo systems as those that have at most three satellites with $V_{\rm max} \geq 30\ {\rm km\,s^{-1}}$, of which at least two have $V_{\rm max} \geq 60\ {\rm km\,s^{-1}}$. In the simulation, the mass distribution of such haloes is wider and shifted towards lower masses, suggesting an MW mass range of $0.25 \leq M_{200}/(10^{12}\ {\rm M_\odot}) \leq 1.4$ at 90 per cent confidence. It is important to note that the low end of the 90 per cent confidence interval, $2.5 \times 10^{11}\ {\rm M_\odot}$, is likely ruled out by observations of the inner part of the Galactic halo. Using the fourth data release of the Radial Velocity Experiment (Kordopatis et al. 2013), Piffl et al. (2014) found that the MW halo mass within 180 kpc is $\geq 9 \times 10^{11}\ {\rm M_\odot}$ at 90 per cent confidence (Smith et al. 2007; Xue et al. 2008; Gnedin et al. 2010; Deason et al. 2012, found similar lower bounds, albeit with larger uncertainties). This result could, in principle, be used as a prior for the kind of analysis we have carried out in this paper, along with other constraints coming from the orbital properties of the massive satellites (e.g. Busha et al. 2011a; González et al. 2013a) or the luminosity function of the nine bright 'classical' dwarf spheroidal satellites (Kennedy et al. 2014, see also Vera-Ciro et al. 2013).

Our results also confirm and extend the conclusion of Wang12 that the TBTF problem highlighted by Boylan-Kolchin et al. (2011b, 2012) is not a problem for the ΛCDM model provided the MW halo mass is close to $1 \times 10^{12}\ {\rm M_\odot}$ rather than to the $\sim 2 \times 10^{12}\ {\rm M_\odot}$ of the Aquarius haloes used in the studies by Boylan-Kolchin et al. Alternative solutions to the problem such as warm dark matter (Lovell et al. 2012), self-interacting dark matter (Vogelsberger, Zavala & Loeb 2012) or baryonic effects (Brooks et al. 2013) are therefore not required unless the mass of the MW halo can be shown to be larger than $\sim 2 \times 10^{12}\ {\rm M_\odot}$.

In our ΛCDM simulations, haloes with a $V_{\rm max}$ distribution similar to that of the MW, that is with at most three satellites with $V_{\rm max} \geq 30\ {\rm km\,s^{-1}}$, of which at least two have $V_{\rm max} \geq 60\ {\rm km\,s^{-1}}$, are rather rare as we have seen in Section 4: at most 1 per cent of haloes of any mass have satellite systems with this property. This shows that the MW lies in the tail of the satellite distribution when analysing the cumulative satellite population at $V_{\rm max,\,1} = 30\ {\rm km\,s^{-1}}$ and $V_{\rm max,\,2} = 60\ {\rm km\,s^{-1}}$, which we call 'the Galactic satellite gap'. However, it is important to note that this result does not necessarily

imply a problem for the ΛCDM paradigm. To asses if the Galactic satellite gap represents a source of tension, we need to calculate what is the probability of finding such a gap in ΛCDM haloes. For this, one needs to search for the presence of satellite gaps not only for $V_{\rm max,\,1} = 30$ km s^{-1} and $V_{\rm max,\,2} = 60$ km s^{-1}, as we did here, but for all possible $V_{\rm max,\,1}$ and $V_{\rm max,\,2}$ combinations. It may be that satellite gaps are quite common, which would suggest that the Galactic satellite gap is a ΛCDM prediction and not a cause of tension.

To assess the robustness of our conclusions, we now explore their sensitivity to various parameters required for this study.

(1) *Cosmological parameters.* The results presented here are based on the MS-II that assumed *WMAP*-1 values for the cosmological parameters. The main difference between these and more recent measurements from *WMAP*-7 (Komatsu et al. 2011) or the *Planck* satellite (Planck Collaboration et al. 2013) is a lower value of σ_8. C14 found that lowering the value of σ_8 from the *WMAP*-1 value of 0.9 to the *WMAP*-7 value of 0.8 results in a slightly lower number of substructures. This translates into a slightly different allowed range for the MW halo mass, as seen from Figs 8 and 9. The probability of finding an MW-like subhalo population assuming *WMAP*-7 parameters (dotted green line in Fig. 9) increases slightly and the peak shifts towards higher masses, but the overall difference is very small. For convenience, we summarized in Table 2 the variations in both the mass estimate and peak height.

(2) *Maximum distance used to identify satellites.* Our analysis so far has been based on substructures found within the virial radius, R_{200}, of the host halo centre. For halo masses of 10^{12} M$_\odot$ and lower, this distance corresponds to $\lesssim$200 kpc and it is significantly smaller than the distances of the outermost known satellites of the MW, such as Leo I, which lies at ∼250 kpc from the halo centre (Karachentsev et al. 2004). To assess the impact of our choice of radius, we repeated the analysis including subhaloes located within a fixed distance of 250 kpc from the host centre, independently on the host mass (see Appendix B for details). The results are shown in Figs 8 and 9 as the dot–dashed red curve that can be compared with the solid curve for our default case. The difference arises because $R_{200} < 250$ kpc for halo masses below 1.5×10^{12} M$_\odot$, which are of interest for our comparison. Since the number of massive substructures increases rapidly with the value of the limiting radius, it becomes more difficult to find haloes with at most three $V_{\rm max} \geq 30$ km s^{-1} subhaloes and this has the effect of lowering the upper limit on the MW halo mass. On the other hand, it becomes easier to find at least two substructures with $V_{\rm max} \geq 60$ km s^{-1} and this has the effect of also lowering the lower limit on the MW haloes mass. The net effect is to shift the allowed mass range to lower values, $0.15 \leq M_{200}/(10^{12}\,{\rm M}_\odot) \leq 1.2$ at 90 per cent confidence, and to reduce the peak probability of finding an MW-like subhalo system.

(3) *Velocity thresholds.* A key ingredient of our analysis are the two velocity thresholds that we use to characterize the MW satellites: 30 km s^{-1} for the threshold above which there should be no more than three subhaloes and 60 km s^{-1} for the threshold above which there should be at least two subhaloes. Increasing the first of these thresholds to 35 km s^{-1} has the effect of weakening the upper limit on the MW halo mass to $M_{200} \lesssim 2.1 \times 10^{12}$ M$_\odot$ (90 per cent confidence; see dash–dotted golden line in Figs 8 and 9). However, decreasing this threshold to 25 km s^{-1} (as suggested by Boylan-Kolchin et al. 2012) has a more dramatic effect (thin-solid purple curve in Figs 8 and 9), giving a mass range of $0.19 \leq M_{200}/(10^{12}\,{\rm M}_\odot) \leq 0.82$ at 90 per cent confidence. The likelihood of finding MW-like subhalo systems for these values of the thresholds varies by factors of a few from the reference case: for the 25 km s^{-1} threshold only ∼0.3 per cent of ΛCDM haloes have such subhalo systems while for a 35 km s^{-1} threshold the probability increases to ∼3 per cent.

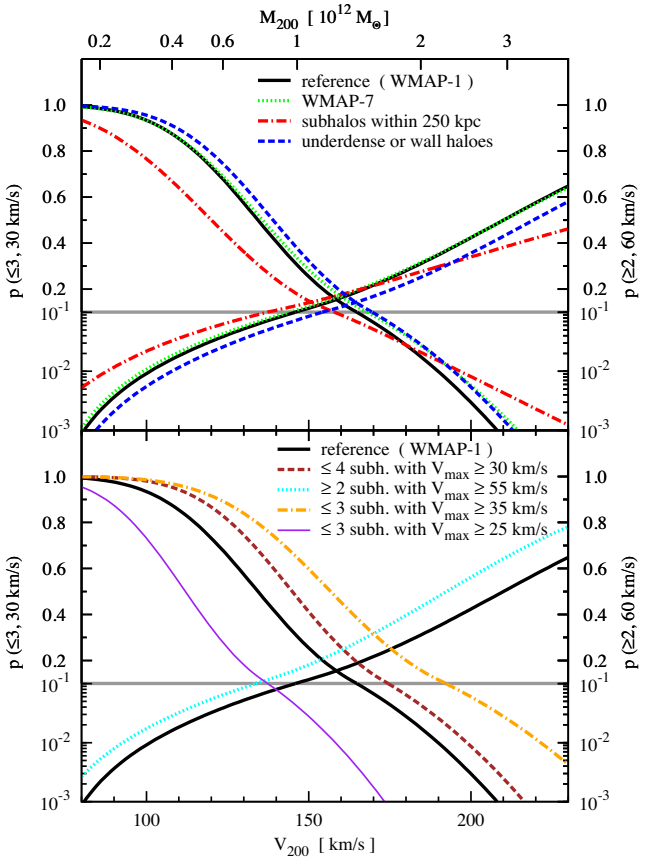

Figure 8. The probability, $p(\leq 3,\ 30\ {\rm km\,s^{-1}})$, that a halo contains at most three subhaloes with $V_{\rm max} \geq 30$ km s^{-1} (left y-axis) and the probability, $p(\geq 2,\ 60\ {\rm km\,s^{-1}})$ that a halo contains at least two subhaloes with $V_{\rm max} \geq 60$ km s^{-1} (right y-axis) as a function of halo virial velocity (lower x-axis) and virial mass (upper x-axis). The lines show the effect of changing some of the assumptions of the reference model studied until now. The solid curves show the reference case of *WMAP*-1 cosmological parameters and substructures found with R_{200} from the host halo centre (as in Figs 2 and 3). Top: results for *WMAP*-7 cosmological parameters (dotted green), predictions when subhaloes within a distance of 250 kpc from the host centre are considered (dash–dotted red) and the effect of large-scale environment by considering only host haloes found in underdense or wall regions (dashed blue). Bottom: outcome of assuming that the MW has four (instead of three; dashed brown) satellites with $V_{\rm max} \geq 30$ km s^{-1}, effect of assuming the MCs have $V_{\rm max} \geq 55$ km s^{-1} (instead of 60 km s^{-1}; dotted cyan) and the results of assuming that the MW has at most three satellites with velocity threshold $V_{\rm max} \geq 35$ km s^{-1} (dash–dotted golden) and $V_{\rm max} \geq 25$ km s^{-1} (thin solid purple), respectively (instead of 30 km s^{-1}). The horizontal grey line shows the 10 per cent level.

Regarding the second velocity threshold, the uncertainties of the best available measurements of the Small MC's rotation velocity are consistent with a value of $V_{\rm max} = 55$ km s^{-1} (Kallivayalil et al. 2013). This change has the effect of slightly weakening the lower limit on the halo mass (dotted cyan curve in Figs 8 and 9). The probability of finding an MW-like subhalo population increases to 1.7 per cent, but the peak position remains unchanged.

Table 2. The sensitivity of the MW mass estimation on the various parameters used in our study. It shows the MW mass range, at 90 per cent confidence, as inferred for the various cases explored in Fig. 8 (third column) and Fig. 9 (fourth column). We also give the peak value (sixth column) and the halo mass at the peak position (fifth column) for each of the data sets shown in Fig. 9.

Data set	Representation in Figs 8 and 9	MW mass limits [$\times 10^{12}$ M$_\odot$] (90 per cent confidence)		Mass at peak position ($\times 10^{12}$ M$_\odot$)	Peak value (per cent)
WMAP-1 reference result	Solid black	1.0–1.4	0.25–1.4	0.61	1.0
WMAP-7 cosmology	Dotted green	1.0–1.6	0.26–1.5	0.64	1.2
Subhaloes within 250 kpc	Dash–dotted red	0.83–1.2	0.15–1.2	0.42	0.80
Underdense or wall haloes	Dashed blue	1.2–1.6	0.28–1.5	0.68	0.83
$\leq$4 subhaloes with $V_{\rm max} \geq 30$ km s^{-1}	Dashed brown	1.0–1.7	0.29–1.5	0.74	2.1
$\geq$2 subhaloes with $V_{\rm max} \geq 55$ km s^{-1}	Dotted cyan	0.77–1.4	0.23–1.3	0.60	1.7
$\leq$3 subhaloes with $V_{\rm max} \geq 35$ km s^{-1}	Dash–dotted golden	1.0–2.3	0.30–2.1	0.93	2.7
$\leq$3 subhaloes with $V_{\rm max} \geq 25$ km s^{-1}	Thin-solid purple	–	0.19–0.82	0.38	0.28

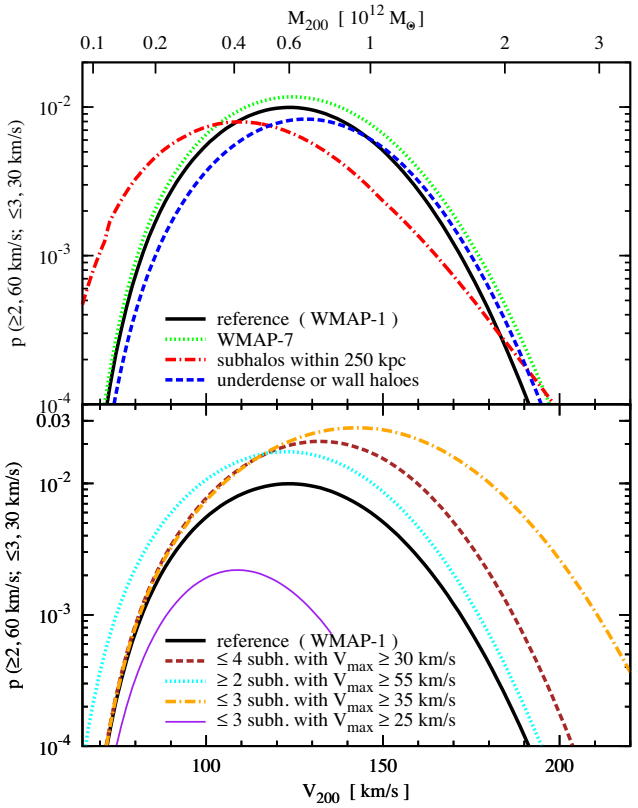

Figure 9. The probability that a halo contains an MW-like subhalo system as a function of halo virial velocity (lower x-axis) or virial mass (upper x-axis). The different lines show the effect of changing some of the assumptions of the reference model studied until now. We explore the same variations from the reference model as in Fig. 8.

In conclusion, our results are most sensitive to the first velocity threshold of 30 km s^{-1}, which is also the one most prone to measurement and modelling uncertainties since it is derived by studying the kinematics of the nine bright 'classical' dwarf spheroidal satellites.

(4) *Incompleteness of MW satellites.* The sample of MW satellites is possibly incomplete, with the recent study of Yniguez et al. (2014) suggesting that around 10 dwarf spherodial satellites await discovery in the area left unexplored by the Sloan Digital Sky Survey. It is possible, though unlikely, that one or more of these undiscovered satellites could have $V_{\rm max} \geq 30$ km s^{-1}. In addition, recent dynamical modelling of the Sculptor dwarf spheroidal galaxy performed by Strigari, Frenk & White (2014) has found that the observational data allow for a maximum circular velocity up to $\sim$35 km s^{-1}. The presence of an additional massive satellite would have the effect of weakening the upper limit on the MW halo mass to $M_{200} \lesssim 1.5 \times 10^{12}$ M$_\odot$ (90 per cent confidence) and increasing the probability of finding an MW-like subhalo system (dashed brown curve in Figs 8 and 9).

(5) *Environmental effects.* Recent studies have shown that the number of substructures depends on the large-scale environment, with haloes in lower density regions having fewer subhaloes (Ishiyama, Fukushige & Makino 2008; Busha et al. 2011b; Croft et al. 2012). This trend has been further quantified by Cautun et al. (in preparation) who find that this effect is significant only for haloes in the most underdense regions and for those residing in the sheets of the cosmic web. These haloes have, on average, 10–20 per cent fewer substructures than the population as a whole, and the deficiency is larger for more massive subhaloes. Environmental effects of this kind may play a role in our galaxy since both observational and theoretical considerations suggest that the Local Group lies within a large-scale sheet (Tully & Fisher 1988; Pasetto & Chiosi 2009; Aragon-Calvo, Silk & Szalay 2011).

To assess the importance of this kind of environmental effect, we have applied NEXUS (Cautun, van de Weygaert & Jones 2013), a morphological environment identification method, to count the substructures of haloes that reside in different environments. The paucity of the most massive subhaloes within wall haloes has the effect of increasing both the lower and upper limits on the allowed MW halo mass (dashed blue curve in Figs 8 and 9) so that the allowed interval shifts to $\sim$10 per cent higher halo masses (see Table 2 for details). The probability of finding an MW-like subhalo system is only slightly lowered.

(6) *Baryonic effects.* Baryonic processes are known to affect the mass function and inner structure of haloes, especially at the low-mass end. For example, Sawala et al. (2013, 2014a) have shown that baryonic effects in simulations of galaxy formation cause haloes with mass $\lesssim 10^{11}$ M$_\odot$ to grow at a reduced rate compared to their counterparts in a dark-matter-only simulation. Baryonic processes also affect the maximum circular velocity of galactic satellites, especially dwarf spheroidal galaxies (e.g. Zolotov et al. 2012; Brooks & Zolotov 2014), which can have important implications for our study. The inclusion of baryons does not affect the maximum circular velocity of massive satellites with $V_{\rm max} \sim 60$ km s^{-1}, but it does lead to an average $\sim$10 per cent reduction in the maximum circular velocity of satellites with $V_{\rm max} \lesssim 30$ km s^{-1} (Sawala et al. in preparation, private communication). These results are based on a

comparison of matched satellites between dark-matter-only and hydrodynamic simulations, in a set of 24 distinct MW mass haloes (The suite of simulations is described in Sawala et al. 2014b). Thus, dwarf spheroidals that have $V_{\rm max} \lesssim 30\ {\rm km\,s^{-1}}$ correspond to subhaloes that, in the dark-matter-only simulations, have a factor of $\sim$1.1 higher maximum circular velocity. This can be easily incorporated into our analysis by changing the condition of finding at most three subhaloes with $V_{\rm max} \geq 30\ {\rm km\,s^{-1}}$ to the conditions of finding at most three subhaloes with $V_{\rm max} \geq 34\ {\rm km\,s^{-1}}$. This weakens the upper limit to the MW halo mass to $M_{200} \lesssim 1.9 \times 10^{12}\,{\rm M}_\odot$ (90 per cent confidence; for clarity we do not show this curve in Figs 8 and 9 but its position can be easily estimated by comparing to the dash–dotted golden line corresponding to $V_{\rm max} \geq 35\ {\rm km\,s^{-1}}$).

6 SUMMARY

We have employed the $V_{\rm max}$ distribution of satellites in the MW to set lower and upper limits to the virial mass of the Galactic halo and to find how likely the MW satellite system is under the assumption that ΛCDM is the correct model for cosmic structure formation. The upper limit comes from requiring that the MW should have at most three subhaloes with $V_{\rm max} \geq 30\ {\rm km\,s^{-1}}$; the lower limit comes from requiring that the MW should have at least two subhaloes with $V_{\rm max} \geq 60\ {\rm km\,s^{-1}}$. The first of these requirements is necessary to avoid the TBTF problem highlighted by Boylan-Kolchin et al. (2011b, 2012), while the second stems from the observation that massive satellites like the MCs are rare (Guo et al. 2011; Lares et al. 2011; Liu et al. 2011).

Our analysis is based on over 10^4 haloes from the Millennium-II simulation. To achieve the required dynamic range, we use an extrapolation method devised by C14 that allows us to count subhaloes down to $V_{\rm max} \sim 15\ {\rm km\,s^{-1}}$. In a first step, we estimate lower and upper bounds to the MW halo mass by treating the number of satellites with $V_{\rm max} \geq 60\ {\rm km\,s^{-1}}$ and those with $V_{\rm max} \geq 30\ {\rm km\,s^{-1}}$ as independent. The former requirement implies an MW mass of $M_{200} \geq 1.0 \times 10^{12}\,{\rm M}_\odot$ while the latter condition indicates that $M_{200} \leq 1.4 \times 10^{12}\,{\rm M}_\odot$, with both limits given at 90 per cent confidence. When requiring that host haloes have a $V_{\rm max}$ distribution similar to that of the MW, that is with at most three satellites with $V_{\rm max} \geq 30\ {\rm km\,s^{-1}}$, of which at least two have $V_{\rm max} \geq 60\ {\rm km\,s^{-1}}$, the allowed mass range becomes $0.25 \leq M_{200}/(10^{12}\,{\rm M}_\odot) \leq 1.4$ (90 per cent confidence).

We also find that the $V_{\rm max}$ distribution of the massive subhaloes of the MW, as defined by the number of satellites with $V_{\rm max} \geq 30\ {\rm km\,s^{-1}}$ and those with $V_{\rm max} \geq 60\ {\rm km\,s^{-1}}$, is quite rare in ΛCDM simulations, with at most $\sim$1 per cent of haloes of any mass having a similar distribution. This might be signalling a tension between the ΛCDM model and observations of the MW satellites, but it is not clear that constructing a solid statistical analysis on such an a posteriori argument is possible without a detailed analysis of the frequency of gaps as a function of the threshold values of $V_{\rm max}$.

Our conclusion regarding the rarity of the MW subhalo system does not vary significantly when we vary the parameters of our model. However, the allowed mass for the MW halo is sensitive to uncertainties in the parameters we use, especially in the $V_{\rm max} = 30\ {\rm km\,s^{-1}}$ threshold that is derived from the kinematics of the nine bright 'classical' dwarf spheroidal satellites. Thus, as pointed out by Wang12 and C14, the TBTF problem is easily avoided if the MW halo has a relatively low mass, certainly within the range of current measurements. However, our study highlights the importance for cosmology of obtaining robust and reliable measurements of the mass of the MW's halo.

ACKNOWLEDGEMENTS

We thank the referee for their useful comments that have improved this paper. We are also grateful to Shaun Cole, Vincent Eke, Douglas Finkbeiner, Julio Navarro, Till Sawala and Andrew Pontzen for helpful discussions and suggestions. This work was supported in part by ERC Advanced Investigator grant COSMIWAY [grant number GA 267291] and the Science and Technology Facilities Council [grant number ST/F001166/1, ST/I00162X/1]. RvdW acknowledges support by the John Templeton Foundation, grant number FP05136-O. WAH is also supported by the Polish National Science Center [grant number DEC-2011/01/D/ST9/01960]. The simulations used in this study were carried out by the Virgo consortium for cosmological simulations. Additional data analysis was performed on the Cosma cluster at ICC in Durham and on the Gemini machines at the Kapteyn Astronomical Institute in Groningen.

This work used the DiRAC Data Centric system at Durham University, operated by ICC on behalf of the STFC DiRAC HPC Facility (www.dirac.ac.uk). This equipment was funded by BIS National E-infrastructure capital grant ST/K00042X/1, STFC capital grant ST/H008519/1, and STFC DiRAC Operations grant ST/K003267/1 and Durham University. DiRAC is part of the National E-Infrastructure. Data from the Millennium/Millennium-II simulation is available on a relational data base accessible from http://galaxy-catalogue.dur.ac.uk:8080/Millennium. This research was carried out with the support of the 'HPC Infrastructure for Grand Challenges of Science and Engineering' Project, co-financed by the European Regional Development Fund under the Innovative Economy Operational Programme.

REFERENCES

Aragon-Calvo M. A., Silk J., Szalay A. S., 2011, MNRAS, 415, L16
Battaglia G. et al., 2005, MNRAS, 364, 433
Behroozi P. S., Wechsler R. H., Wu H.-Y., 2013, ApJ, 762, 109
Benson A. J., Frenk C. S., Lacey C. G., Baugh C. M., Cole S., 2002, MNRAS, 333, 177
Boylan-Kolchin M., Springel V., White S. D. M., Jenkins A., Lemson G., 2009, MNRAS, 398, 1150
Boylan-Kolchin M., Springel V., White S. D. M., Jenkins A., 2010, MNRAS, 406, 896
Boylan-Kolchin M., Besla G., Hernquist L., 2011a, MNRAS, 414, 1560
Boylan-Kolchin M., Bullock J. S., Kaplinghat M., 2011b, MNRAS, 415, L40
Boylan-Kolchin M., Bullock J. S., Kaplinghat M., 2012, MNRAS, 422, 1203
Brooks A. M., Zolotov A., 2014, ApJ, 786, 87
Brooks A. M., Kuhlen M., Zolotov A., Hooper D., 2013, ApJ, 765, 22
Busha M. T., Marshall P. J., Wechsler R. H., Klypin A., Primack J., 2011a, ApJ, 743, 40
Busha M. T., Wechsler R. H., Behroozi P. S., Gerke B. F., Klypin A. A., Primack J. R., 2011b, ApJ, 743, 117
Cautun M., van de Weygaert R., Jones B. J. T., 2013, MNRAS, 429, 1286
Cautun M., Frenk C. S., van de Weygaert R., Hellwing W. A., Jones B. J. T., 2014, preprint (arXiv:1405.7697), (C14)
Croft R. A. C., Matteo T. D., Khandai N., Springel V., Jana A., Gardner J. P., 2012, MNRAS, 425, 2766
Deason A. J. et al., 2012, MNRAS, 425, 2840
Dehnen W., McLaughlin D. E., Sachania J., 2006, MNRAS, 369, 1688
Diaz J. D., Koposov S. E., Irwin M., Belokurov V., Evans W., 2014, MNRAS, 443, 1688
Diemand J., Kuhlen M., Madau P., Zemp M., Moore B., Potter D., Stadel J., 2008, Nature, 454, 735
Gnedin O. Y., Brown W. R., Geller M. J., Kenyon S. J., 2010, ApJ, 720, L108
González R. E., Kravtsov A. V., Gnedin N. Y., 2013, ApJ, 770, 96

González R. E., Kravtsov A. V., Gnedin N. Y., 2014, ApJ, 773, 91
Grebel E. K., 2005, in Jerjen H., Binggeli B., eds, IAU Colloq. 198: Near-Fields Cosmology with Dwarf Elliptical Galaxies. Cambridge Univ. Press, Cambridge, p. 1
Guo Q., White S., Li C., Boylan-Kolchin M., 2010, MNRAS, 404, 1111
Guo Q., Cole S., Eke V., Frenk C., 2011, MNRAS, 417, 370
Harris J., Zaritsky D., 2006, AJ, 131, 2514
Ishiyama T., Fukushige T., Makino J., 2008, PASJ, 60, L13
Kallivayalil N., van der Marel R. P., Besla G., Anderson J., Alcock C., 2013, ApJ, 764, 161
Karachentsev I. D., Karachentseva V. E., Huchtmeier W. K., Makarov D. I., 2004, AJ, 127, 2031
Kennedy R., Frenk C., Cole S., Benson A., 2014, MNRAS, 442, 2487
Klypin A., Kravtsov A. V., Valenzuela O., Prada F., 1999, ApJ, 522, 82
Klypin A. A., Trujillo-Gomez S., Primack J., 2011, ApJ, 740, 102
Komatsu E. et al., 2011, ApJS, 192, 18
Kordopatis G. et al., 2013, AJ, 146, 134
Kravtsov A. V., Berlind A. A., Wechsler R. H., Klypin A. A., Gottlöber S., Allgood B., Primack J. R., 2004, ApJ, 609, 35
Lares M., Lambas D. G., Domínguez M. J., 2011, AJ, 142, 13
Liu L., Gerke B. F., Wechsler R. H., Behroozi P. S., Busha M. T., 2011, ApJ, 733, 62
Łokas E. L., 2009, MNRAS, 394, L102
Lovell M. R. et al., 2012, MNRAS, 420, 2318
Madau P., Diemand J., Kuhlen M., 2008, ApJ, 679, 1260
Moore B., Ghigna S., Governato F., Lake G., Quinn T., Stadel J., Tozzi P., 1999, ApJ, 524, L19
Olsen K. A. G., Massey P., 2007, ApJ, 656, L61
Onions J. et al., 2012, MNRAS, 423, 1200
Parry O. H., Eke V. R., Frenk C. S., Okamoto T., 2012, MNRAS, 419, 3304
Pasetto S., Chiosi C., 2009, A&A, 499, 385
Peñarrubia J., McConnachie A. W., Navarro J. F., 2008, ApJ, 672, 904
Piffl T. et al., 2014, A&A, 562, A91
Planck Collaboration et al., 2013, preprint (arXiv:1303.5076)
Purcell C. W., Zentner A. R., 2012, J. Cosmol. Astropart. Phys., 12, 7
Sawala T., Frenk C. S., Crain R. A., Jenkins A., Schaye J., Theuns T., Zavala J., 2013, MNRAS, 431, 1366
Sawala T. et al., 2014a, preprint (arXiv:1404.3724)
Sawala T. et al., 2014b, preprint (arXiv:1406.6362)
Smith M. C. et al., 2007, MNRAS, 379, 755
Spergel D. N. et al., 2003, ApJS, 148, 175
Springel V. et al., 2005, Nature, 435, 629
Springel V. et al., 2008, MNRAS, 391, 1685
Stadel J., Potter D., Moore B., Diemand J., Madau P., Zemp M., Kuhlen M., Quilis V., 2009, MNRAS, 398, L21
Stanimirović S., Staveley-Smith L., Jones P. A., 2004, ApJ, 604, 176
Strigari L. E., Bullock J. S., Kaplinghat M., Simon J. D., Geha M., Willman B., Walker M. G., 2008, Nature, 454, 1096
Strigari L. E., Frenk C. S., White S. D. M., 2010, MNRAS, 408, 2364
Strigari L. E., Frenk C. S., White S. D. M., 2014, preprint (arXiv:1406.6079)
Tully R. B., Fisher J. R., 1988, Catalog of Nearby Galaxies. Cambridge Univ. Press, Cambridge
van der Marel R. P., Kallivayalil N., 2014, ApJ, 781, 121
van der Marel R. P., Alves D. R., Hardy E., Suntzeff N. B., 2002, AJ, 124, 2639
Vera-Ciro C. A., Helmi A., Starkenburg E., Breddels M. A., 2013, MNRAS, 428, 1696
Vogelsberger M., Zavala J., Loeb A., 2012, MNRAS, 423, 3740
Walker M. G., Mateo M., Olszewski E. W., Peñarrubia J., Wyn Evans N., Gilmore G., 2009, ApJ, 704, 1274
Wang J., Frenk C. S., Navarro J. F., Gao L., Sawala T., 2012, MNRAS, 424, 2715 (Wang12)
Watkins L. L., Evans N. W., An J. H., 2010, MNRAS, 406, 264
Weinberg D. H., Colombi S., Davé R., Katz N., 2008, ApJ, 678, 6
Willman B. et al., 2005, ApJ, 626, L85
Wolf J., Martinez G. D., Bullock J. S., Kaplinghat M., Geha M., Muñoz R. R., Simon J. D., Avedo F. F., 2010, MNRAS, 406, 1220
Xue X. X. et al., 2008, ApJ, 684, 1143
Yniguez B., Garrison-Kimmel S., Boylan-Kolchin M., Bullock J. S., 2014, MNRAS, 439, 73
Zheng Z. et al., 2005, ApJ, 633, 791
Zolotov A. et al., 2012, ApJ, 761, 71

APPENDIX A: THE PROBABILITY OF FINDING MW-LIKE SATELLITES

Here, we give a detailed description of the model that we use to predict the probability, $p(\geq X_1, V_1; \leq X_2, V_2)$, that a halo contains at least X_1 subhaloes with $V_{\rm max} \geq V_1$ and at most X_2 substructures with $V_{\rm max} \geq V_2$, where $V_1 \geq V_2$. For simplicity, we use the notation

$$\mathcal{P} = p(\geq X_1, V_1; \leq X_2, V_2) \tag{A1}$$

and we take $X_2 \geq X_1$. The case $X_2 < X_1$ is trivial since the probability is zero.

In the first instance, we restrict attention to host haloes with virial velocity, V_{200}. Using the notation,

$$\nu_1 = \frac{V_1}{V_{200}} \quad \text{and} \quad \nu_2 = \frac{V_2}{V_{200}}\,, \tag{A2}$$

the probability $\mathcal{P}$ reduces to finding all the haloes with V_{200} that contain at least X_1 subhaloes with $\nu \geq \nu_1$ and at most X_2 subhaloes with $\nu \geq \nu_2$. At ν_2 there are, on average,

$$\Delta N = \overline{N}(>\nu_2) - \overline{N}(>\nu_1) \tag{A3}$$

more substructures per halo than at ν_1, where $\overline{N}(>\nu_1)$ and $\overline{N}(>\nu_2)$ are the mean subhalo counts at those two velocity ratios. We make the assumption that these subhaloes with $\nu \in [\nu_2, \nu_1]$ are distributed among the host population according to a Poisson distribution with mean ΔN that is independent on the number of substructures at ν_1. Therefore, a halo has a probability,

$$P_{\rm Poisson}(l, \Delta N) = \frac{\Delta N^l}{l!} {\rm e}^{-\Delta N}, \tag{A4}$$

of having l subhaloes with $\nu \in [\nu_2, \nu_1]$. The same halo has probability

$$P_{\rm Poisson}(\leq i, \Delta N) = \sum_{l=0}^{i} \frac{\Delta N^l}{l!} {\rm e}^{-\Delta N} \tag{A5}$$

of having at most i substructures in the range $[\nu_2, \nu_1]$.

The only haloes that contribute to $\mathcal{P}$ are those that have between X_1 and X_2 substructures with $\nu \geq \nu_1$. Let us select such a halo containing $k \in [X_1, X_2]$ subhaloes with $\nu \geq \nu_1$. This halo can contribute to $\mathcal{P}$ only if it has at most X_2 substructures with $\nu \geq \nu_2$ and therefore it can have at most $X_2 - k$ subhaloes in the range $[\nu_2, \nu_1]$. The probability that it satisfies this condition is given by equation (A5) with $i = X_2 - k$.

The quantity, $\mathcal{P}$, is given by the fraction of haloes with k substructures at $\nu \geq \nu_1$ times the probability that they contain less than $X_2 - k$ subhaloes in the range $[\nu_2, \nu_1]$, summed over k. Therefore, we have

$$\mathcal{P} = \sum_{k=X_1}^{X_2} P(k|r(>\nu_1), s(>\nu_1))\; P_{\rm Poisson}(\leq X_2 - k, \Delta N)\,, \tag{A6}$$

where $P(k|r(>\nu_1), s(>\nu_1))$ is the negative binomial distribution that gives the probability that a halo has k substructures with $\nu > \nu_1$ (see equations 2 and 3). The probability, $\mathcal{P}$, is a function of halo virial velocity, or equivalently, halo mass, through the dependence of r and s on ν_1 as well as the variation of ΔN with ν_1 and ν_2.

APPENDIX B: THE SUBHALO ABUNDANCE WITHIN A FIXED PHYSICAL RADIUS

To compute the subhalo abundance within a fixed physical radius, we make use of the universality of $\overline{N}(>\nu)$ with host halo mass. This approximation is valid when $\overline{N}(>\nu)$ is measured within a distance fR_{200}, with f a multiplication factor. This is illustrated in Fig. 4 for a value of $f = 1$. We have checked that the universality still applies, to within $\sim$20 per cent, for the mass range $1 \times 10^{11}\,\mathrm{M}_{\odot} \leq M_{200} \leq 1 \times 10^{13}\,\mathrm{M}_{\odot}$, for values of f in the range $0.5 \leq f \leq 3.0$.

Computing the subhalo abundance within a fixed physical radius, R, is equivalent to a distance, fR_{200}, with

$$f \equiv \frac{R}{R_{200}} \,. \tag{B1}$$

Since R_{200} is a function of mass, the multiplication factor, f, is itself a function of halo mass, with f decreasing with increasing halo mass. We computed the subhalo abundance within a distance of fR_{200} for a set of f values in the range 0.57–2.7, which corresponds to a fixed distance of $R = 250\,\mathrm{kpc}$ spanning the mass range $1 \times 10^{11}\,\mathrm{M}_{\odot} \leq M_{200} \leq 1 \times 10^{13}\,\mathrm{M}_{\odot}$. The f values were selected to give nine equally spaced bins in M_{200}. Following this, the abundance of subhaloes at a given halo mass was found using a linear interpolation between the results for the two closest values of f corresponding to that mass value.

This paper has been typeset from a TEX/LATEX file prepared by the author.